Rapid scan absorption spectroscopy using a waveform-driven electro-optic phase modulator in the 1.6–1.65 μm region

Kevin O. Douglass,[1] Stephen E. Maxwell,[2] Gar-Wing Truong,[3] Roger D. van Zee,[3] James R. Whetstone,[4] Joseph T. Hodges,[3] David A. Long,[3] and David F. Plusquellic[1,*]

[1]*Quantum Electronics and Photonics Division, Physical Measurement Laboratory, National Institute of Standards and Technology, Boulder, Colorado 80305, USA*

[2]*Sensor Science Division, Physical Measurement Laboratory, National Institute of Standards and Technology, Gaithersburg, Maryland 20899, USA*

[3]*Chemical Sciences Division, Material Measurement Laboratory, National Institute of Standards and Technology, Gaithersburg, Maryland 20899, USA*

[4]*Office of Special Programs, National Institute of Standards and Technology, Gaithersburg, Maryland 20899, USA*

**Corresponding author: david.plusquellic@nist.gov*

Received May 21, 2013; accepted August 17, 2013;
posted August 29, 2013 (Doc. ID 190921); published September 25, 2013

A method is reported for performing fast optical frequency scans over a bandwidth of 36.9 GHz and at a sweep rate of 40 kHz using a single second-order sideband from an electro-optic phase modulator driven by an arbitrary waveform generator. Single sideband selection is accomplished using the resonator modes of a Fabry–Perot filter cavity having a finesse of ≈44 and a free-spectral range of 300 MHz. The finesse is sufficiently high to give <2% total transmission of the laser frequency carrier and all other nonresonant sidebands while sufficiently low to ensure on-resonance switching times as short as 100 ns. A frequency offset component of a diode laser is used for active stabilization of the laser to the filter cavity at all times eliminating frequency drift of the filter cavity transmission comb used for single sideband selection and scanning. The method is demonstrated for the detection of CO_2 near 1602 nm and for CH_4 lines near 1643 nm. Detection of ambient level concentrations of each of these gases is demonstrated in a 25 μs scan over a path length of 50 m at a sensitivity of $\approx 3 \times 10^{-9}$ $cm^{-1}\,Hz^{-1/2}$. The corresponding measurement uncertainties ($k = 1$ or 1σ) in a (2–3) ms time period and a 1 km path length are $< \pm 2$ μmol/mol (ppm) for CO_2 and $< \pm 5$ nmol/mol (ppb) for CH_4. The arbitrary waveform control of the pulse sequence, repetition rate, and duty cycle provides for optimization of the light source for a variety of application areas that include path integrated differential absorption and differential absorption light detection and ranging.

OCIS codes: (280.3420) Laser sensors; (280.1910) DIAL, differential absorption lidar; (280.4788) Optical sensing and sensors; (300.6340) Spectroscopy, infrared; (250.7360) Waveguide modulators.

http://dx.doi.org/10.1364/JOSAB.30.002696

1. INTRODUCTION

Direct absorption spectroscopy is one of the most important methods in the determination of analyte concentration in gases, liquids, and solids and is employed across a wide range of applications in laboratory science and remote sensing. The application of cavity-enhanced methods [1] to increase absorption paths to kilometer length scales is among the most direct ways to enhance absorption sensitivity. Indeed, cavity ring-down spectroscopy (CRDS) [2–4] and noise-immune cavity-enhanced optical heterodyne molecular spectroscopy (NICE-OHMS) [5–9] that use resonator cavities equipped with high-reflectivity (low-loss) mirrors are among the most sensitive methods reported to date. A significant advantage realized in NICE-OHMS is the immunity of the measurement to amplitude noise from frequency jitter of the laser source relative to the cavity, and in CRDS, to the amplitude noise of the source itself. In CRDS, the absorption rate of a sample is obtained directly from the change in the optical decay rate of the pumped cavity mode. Meanwhile, in NICE-OHMS, absorption derived from dispersion is determined from demodulation of the frequency sidebands and carrier, all resonant with the cavity [5]. When considering only methods that are widely tunable, absorption sensitivities that approach 10^{-11} $cm^{-1}\,Hz^{-1/2}$ are well documented [4,6–8]. Based on a method similar to that presented in [10], we have recently reported a sensitivity of 2×10^{-12} $cm^{-1}\,Hz^{-1/2}$ using a new CRDS method to perform frequency-agile rapid scanning spectroscopy (FARS) [11,12] with an electro-optic phase modulator (EOM).

A disadvantage of cavity-enhanced methods is the need to couple light into a narrow cavity resonance often only a few kilohertz in width. Consequently, frequency fluctuations of the resonator mode from pressure and temperature changes in the optical path length often preclude the use of open-to-atmosphere resonators. Furthermore, cavity-enhanced methods require insertion of the sample between the resonator mirrors, which is not feasible for applications such as remote sensing. Multipass cells [13,14] and open-path absorption measurements [15] provide alternatives to high-finesse cavities without the severe stability requirements. Dual-beam methods that ratio the signal and reference powers to minimize common mode source noise are shown to achieve the highest

levels of sensitivity [16]. In well-controlled laboratory environments, near-shot-noise-limited performance is widely reported in multipass cells [16–19]. However, remote sensing techniques require optical paths open to the atmosphere where absorption sensitivity can be significantly degraded because of changing conditions. For example, the path integrated absorption signal can fluctuate during the course of a scan on the millisecond time scale [20–22] from changes in analyte concentration and aerosol scattering density or from pressure gradients that induce beam positioning jitter at the receiver. Such effects can be minimized if the time to scan across the feature or features of interest is faster than the time scale for atmospheric changes. As such, each spectral scan can float on top of a varying baseline given by the signal-to-reference-power ratio with little impact on the absorption feature. Even when used with multipass cell techniques as we show below, fast spectral scans are advantageous for capturing a snapshot of the magnitude and phase of standing wave interference patterns or other geometry-dependent variations before path length drift can occur across the spectral region of interest.

A second important consideration when targeting the optimal signal to noise at the receiver is the spectral coverage required. Most commercial lasers regardless of pulse duration deliver an average power in the range of (1–10) W. Since the best possible signal-to-noise ratio (S/N) for power law detectors scales with $N^{-1/2}$ where N is the number of detected photons, it is advantageous to keep the spectral region as narrow as possible. This is particularly important for differential absorption light detection and ranging (DIAL) techniques in which detection limits from aerosol scattering are nearly always limited by the photon flux at the receiver [22–24]. For the remote detection of a single atmospheric species at ambient pressure, the spectral range required can be as small as 10 GHz.

It is with these considerations in mind that we report a near-infrared technique to perform rapid and continuously repeatable scans at a rate that is nearly two orders of magnitude faster than the millisecond time scale associated with atmospheric changes. Specifically, the method allows for rapid step frequency scans at 300 MHz intervals and a step rate of 5×10^6/s and permits scans over a spectral interval of ≈40 GHz on a time scale of 25 μs/scan without the need to tune the laser. The scan repetition rate of 40 kHz is accomplished using a 24 gigasample/s (GS/s) arbitrary waveform generator (AWG) coupled to a high-bandwidth waveguide-based EOM to generate a series of sidebands on the output of a single-frequency external-cavity diode laser. A single sideband of given order and phase is generated for transmission through a medium-finesse Fabry–Perot resonator. The finesse is chosen to achieve the necessary spectral purity while permitting a rapid temporal response with high transmission power for detection. In this work, we demonstrate detection of ambient levels of CH_4 and CO_2 in a 25 μs scan time over a ≈50 m path length in a White cell. We also show the ability to rapidly monitor CH_4 at ambient levels over 5 ms time windows under steady flow conditions through the White cell at atmospheric pressure. The short scan times that effectively sample "frozen" atmospheric conditions are expected to significantly reduce retrieval errors in the concentration profiles.

2. EXPERIMENTAL METHODS

The experimental arrangement is shown in Fig. 1. The principal components of the system consist of an external-cavity single-frequency diode laser, a medium-finesse Fabry–Perot confocal cavity (filter cavity) for single sideband selection, an EOM driven by an AWG having 12 GHz of bandwidth, and a long-pass White cell aligned for ≈50 m path length [10]. The diode laser is fiber coupled through an optical isolator and then amplified to 20 mW using a booster amplifier. The output is split into two paths using a 70%/30% fiber splitter with the 70% path used for high-speed scanning and the 30% path used for stabilization of the diode laser and filter cavity [10,12].

The 30% leg is fiber coupled to a waveguide-based EOM to add 15 MHz sidebands for use in the stabilization loops discussed below. The output is fiber coupled to an acousto-optic modulator (AOM) driven near its center frequency of 250 MHz using a tunable RF source referenced to a 10 MHz Rb source. The first-order (+) sideband is tunable over ±30 MHz with >5% efficiency and fiber coupled to a three-port optical circulator. The output is propagated in free space through a polarizing beam splitter (PBS) and then slightly off-axis coupled to the filter cavity. The signal from a 150 MHz bandwidth photodiode that monitors the reflected beam from the circulator is mixed with the 15 MHz reference and demodulated for stabilization using the Pound–Drever–Hall (PDH) technique [25]. The PDH error signal is conditioned in a 10 MHz band-pass proportional/integral (PI) gain controller, and its output provides direct feedback to the diode laser current for stabilization to the filter cavity. The input for diode laser current modulation is DC coupled and limited to 1 MHz. The lock

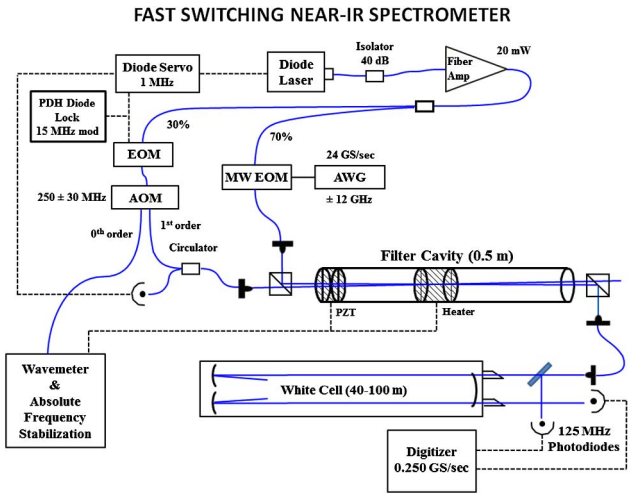

Fig. 1. Schematic of the fast switching laser spectrometer. The amplified diode laser output is split into two paths for active stabilization of the filter cavity for single sideband transmission. The 30% path (lock path) is used for active stabilization of the diode laser to the filter cavity using an EOM ($\Delta\nu_{\mathrm{mod}} \pm 15$ MHz) for generation of a PDH feedback signal and an AOM (250 MHz ± 30 MHz) for offset shifting the carrier relative to the scan leg. The 70% path (scan path) includes a broadband EOM (MW EOM) driven by a 12 GHz bandwidth AWG to add tunable sidebands, only one of which is resonant with a filter cavity mode. The transmitted sideband is free-space coupled into a long-pass White cell with typical path lengths from 40 to 100 m. Two InGaAs photodiodes (125 MHz bandwidth) and an 8-bit digital oscilloscope are used to simultaneously measure the absorption signal and reference power at each step of the AWG (see text for additional details).

stability of the laser relative to the filter cavity is estimated to be better than 400 kHz from the root-mean-square noise content of the error signal.

The 70% path is fiber coupled to a second waveguide-based EOM driven by an AWG. Two channels of the AWG are interleaved to give a 24 GS/s clock rate having nearly 12 GHz of bandwidth. The AWG has a maximum waveform output of 0.7 V_{pp}. As discussed below, it is desirable to drive the phase modulator with up to π rad of phase shift where the second-order sideband is near its peak in relative amplitude. To achieve this condition, the AWG is amplified by 24 dB in a (0.1–12) GHz amplifier. The EOM output is propagated in free space through a PBS and mode matched to the filter cavity. To improve the portability of the system and output beam quality, the transmitted sideband is coupled into a single-mode fiber and then launched for free-space coupling to the White cell. Prior to entrance to the cell, a portion of the power similar in magnitude to the transmitted power through the cell is sampled for normalization purposes. The overall throughput efficiency of the filter cavity is ≈5%.

The continuous-wave signals reflected from and transmitted through the filter cavity are illustrated in Fig. 2. The signals were measured as the laser was scanned to lower frequency for a fixed cavity length. The filter cavity is a 0.5 m confocal resonator having a transverse mode spacing, $\Delta\nu_{MS}$, of 150 MHz. The top trace is the reflected cavity signal of the lock path where each reflection dip at a cavity resonance has ±15 MHz sidebands appearing as shoulders. The cavity transmission of the scan path is shown as the lower trace with the EOM driving field turned off. The frequency offset relative to the lock path is a result of the AOM shift of 250 MHz.

The middle trace in Fig. 2 is the filter transmission of the scan path when a 50 MHz continuous-wave signal from the AWG is applied to the EOM. Under these conditions, only the negative second-order sideband is resonant while the other second-order, two first-order, and two third-order sidebands and diode laser (carrier) signals are rejected (i.e., reflected). For a confocal resonator with mode spacing, $\Delta\nu_{MS}$, the diode laser offset frequency, $\delta \cdot \Delta\nu_{MS}$, for transmission of a resonant sideband of order O_R may be determined according to

$$\delta \cdot \Delta\nu_{MS} = [O_R/(2O_R - O_L + O_H)]\Delta\nu_{MS}, \tag{1}$$

where O_L and O_H are the lowest- through the highest-order sidebands to reject. In the case of Fig. 2, $O_R = 2$, $O_L = 1$ and $O_H = 3$ to give $1/3 \cdot \Delta\nu_{MS}$ or 50 MHz. This formulation assumes that power in the $O_H + 1$ is negligible as this order will be resonant. It is further noted that by subtracting 0.5 from the denominator in Eq. (1), the order, O_H, for sideband rejection will be doubled at the cost of halving the frequency difference between a cavity resonance and the two lower-order sidebands, O_H and $O_H + 1$. Further improvements in spectral purity may be realized by accounting for the Bessel function power distribution of the EOM response.

Once δ is determined, the AWG is programmed with two series of frequencies separated by the desired frequency step, $\Delta\nu_{FS} = n\Delta\nu_{MS}$ (for integer n), according to

$$\nu_{EO}^{+}(i) = [(\delta/O_R + i)/O_R]\Delta\nu_{FS}, \tag{2a}$$

$$\nu_{EO}^{-}(i) = [(1 - \delta/O_R + i)/O_R]\Delta\nu_{FS}, \tag{2b}$$

where $\nu_{EO}^{+}(i)$ and $\nu_{EO}^{-}(i)$ are the transmitted positive and negative sideband frequency branches, respectively, for $i = 0$ to the maximum microwave frequency.

While higher-finesse cavities quickly improve the spectral purity as given by the Airy transmission function for a given cavity length, this property also increases the cavity response time. For this reason, a cavity finesse of ≈44 is chosen for this application. The measured spectral purity versus switching speed is illustrated in Fig. 3. The measured diode laser transmission in the scan path when offset by 50 MHz is 1.2%, in

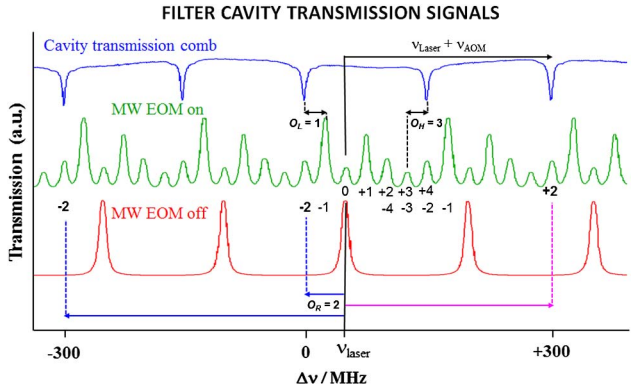

Fig. 2. Signals transmitted by the filter cavity as the laser is scanned from high to low frequency (or cavity from low to high frequency). The top trace is the lock path signal that is reflected from the filter cavity, with each reflection dip having small shoulders associated with 15 MHz modulation used for stabilization purposes. The lower trace is scan path transmission without EOM sidebands. It is shifted from the lock path signal by the AOM frequency of 250 MHz. The middle trace is the scan path with EOM sidebands driven at one of the MW frequencies generated by the AWG. The sideband pulses are rapidly scanned and transmitted through the filter cavity at frequencies indicated with vertical lines for the plus and minus sideband series.

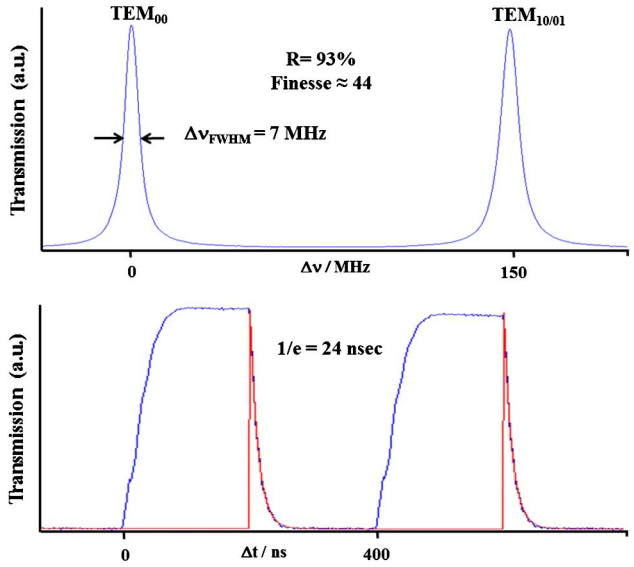

Fig. 3. Measured transmission of the filter cavity (top panel) of the scan path (without sidebands) and the temporal response of the filter cavity when the EOM is driven with 400 ns long microwave pulses from the AWG. The pulse length is four times longer than that used for the fast scans below in order to illustrate the full exponential decay.

good agreement with the Airy function predictions at this finesse. To assess switching speed, the measured temporal response of the cavity following a square wave input pulse to the EOM is shown in the lower panel. The fitted decay constant, τ, is 24 ns, which is within 6% of the value from the time-bandwidth product, $(2\pi\Delta\nu_{\mathrm{FWHM}})^{-1}$, expected for the 7 MHz full width at half-maximum (FWHM) of the transmission peak. These properties also indicate that the switching times associated with the AWG electronics and EOM are short in comparison.

The V_π phase shift condition of the EOM increases by a factor of ≈1.5 from 1 to 10 GHz. Other standing wave issues (optical or electrical) may also lead to slight variations in the sideband power delivered by the EOM. The digital amplitude control of the AWG waveforms with (8 or 10) bit resolution is convenient for power leveling purposes. Power leveling has the obvious advantage for direct absorption detection where the impact of problems with reference power normalization is minimized. The leveling of sideband power across each of the stepped microwave frequencies is performed in a two-step process. First, the Bessel function distribution of the transmitted sideband amplitudes at each frequency step is determined by delivering a series of linearly increasing microwave voltages and integrating across the optical signal pulses of the reference detector at each step. A reasonable reference amplitude is selected, and at each frequency step, an estimate of the lowest microwave voltage to achieve this reference level is obtained from interpolation over the measured calibration curve. The calibration curves are found to provide adequate initial voltages at any diode laser frequency across its full tuning range (1597–1645 nm). Further refinements to the microwave driving voltages are performed in a few seconds by integrating the optical signal powers, P_i, at each driving frequency and adjusting the waveform amplitudes, $A_{MW}(i)$, in a nonlinear way according to

$$A_{MW}(i) = [(P_{\mathrm{damp}} + P_{\mathrm{average}})/(P_{\mathrm{damp}} + P_i)]^{1/2}, \qquad (3)$$

where P_{damp} is typically chosen to be less than half the average integrated signal, P_{average}. The power flatness is typically better than 2% across nearly the full tuning range after a few iterations except for pulses near the highest EOM driving frequencies that fall below the reference level (see lower panel of Fig. 4).

For long-term measurements that extend beyond 10 min, it is advantageous to provide an absolute frequency reference for the diode laser. This is achieved by locking the zero-order beam from the AOM (with 15 MHz sidebands) to an optical transfer cavity [26]. The transfer cavity is actively locked to a polarization-stabilized HeNe laser using a piezoelectro transducer (PZT) and heater [27] and is known from prior work to have a long-term absolute frequency stability of better than ±0.5 MHz [28]. Since the laser is frequency locked to the filter cavity, slow feedback corrections (with a 0.1 s time constant) to the laser frequency are indirectly enforced by controlling the filter cavity length using the PZT and a low-noise, high-voltage amplifier.

3. RESULTS AND DISCUSSION

The objective of this study is to demonstrate a sensitive direct absorption method to perform fast and precise frequency

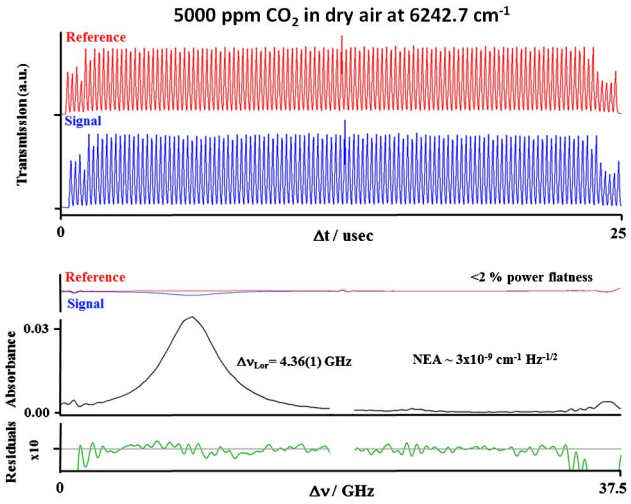

Fig. 4. Measured absorption signals of a gas mixture of 5000 μmol/mol CO_2 (≈13 times ambient level) in dry air in a White cell path length of 44.6(6) m and at atmospheric pressure. The top panel illustrates the raw time domain signals measured on the reference detector (top trace) and signal detector (lower trace) with each sideband pulse on for 100 ns and then off for 100 ns for 123 pulses. Each scan makes use of the second-order sidebands with a frequency step size of 300 MHz and covers 36.9 GHz in 25 μs. The top two traces in the lower panel show the integrated signals from the reference and signal channels. The power in the reference channel is leveled according to the procedure described in the text, and variations are less than 2% (except near the ends of the scan). The small break in the center of the scan is from the removal of three points where heterodyne signals are observed from the small leakage of the diode laser carrier. The absorbance spectrum is shown in the lower panel after subtraction of three etalon fringe components and base line (see text for details). The residuals from a Voigt profile fit are shown as the lowest trace. A small feature (<1% of the main line) included in the fit at 23.3 GHz is from fourth-order leakage as verified by the relative linewidth value of ≈1/2.

scans over a spectral region large enough to capture the on- and off-resonance regions of CO_2 and CH_4 lines in the open atmosphere. At atmospheric pressure, the typical FWHM of CO_2 lines near 1.60 μm is ≈4 GHz, and it is somewhat larger for CH_4 (≈6 GHz) because of its additional Coriolis-induced structure. Therefore, a minimum coverage of 20–30 GHz is needed to ensure reliable baselines for quantitative absorption measurements. Since the Nyquist-limited bandwidth of the AWG is 12 GHz for 24 GHz of tuning using the two sidebands, doubling this frequency range would provide a sufficient baseline for each greenhouse gas. Therefore, the EOM of the scan path was optimized for second-order sideband transmission through the filter cavity. In Eq. (1), $\delta = 1/3$ was used to offset the diode frequency in the scan path by 50 MHz relative to a transmission fringe of the cavity. The frequency step size, $\Delta\nu_{\mathrm{FS}}$, of 300 MHz was chosen to give (10–20) points across the FWHM of the lines of interest. The AWG was programmed with two series of pulses beginning with the negative sideband at 9.175 GHz and decreasing to 0.175 GHz (61 pulses) and then with the positive sideband beginning at 0.025 GHz and increasing to 9.125 GHz (62 pulses). The microwave power at each frequency was turned on for 100 ns followed by 100 ns off time before switching frequencies. The on/off time of 100 ns corresponds to four time constants of the ring-down time of the filter cavity (see Fig. 3). Over the 200 ns period, about 50% of the full power is recovered in 180 ns integration intervals, and less than 5% of the residual light leaks into the next

frequency interval. The entire pulse sequence consists of 123 steps, covers a 36.9 GHz region, and is completed in 25 μs corresponding to a 1500 THz/s scan rate. It is further noted that any scan sequence is possible using the AWG (including random ones), which may be useful in some cases for signal averaging over time correlated noise sources.

Full control and generation of the pulse sequence waveform is performed on a computer and transferred to the AWG using a general purpose interface bus (GPIB) interface. The record length is only 0.6 MS (for a single scan pattern) at the full interleaved clock rate of 24 GS/s, and the waveform transfer time is less than a few seconds. Once loaded on the AWG, the 25 μs pulse sequence is replayed at the full repetition rate of 40 kHz.

The reference and sample signals were digitized on an 8-bit oscilloscope at twice the detector bandwidth (250 MHz). The typical record length before transfer to the computer was 12.5 MS/channel and consists of 2000 scans acquired in 50 ms. The scope-to-computer transfer was performed using a four-lane peripheral component interconnect express (PCIe) controller and requires about 0.74 s/record. The throughput is thus a factor of 15 slower than the maximum experimental repetition rate of 40 kHz.

A. Direct Absorption of CO_2 Near 1.602 μm

The signal-averaged data of CO_2 at 6242.666 cm^{-1} (30013-00001 R20e line [29]) from a 50 ms (2000 scan sequence) are shown in Fig. 4. For this measurement, the White cell was filled to ≈99 kPa (740 Torr) with a premixed gas sample consisting of 5000 μmol/mol (ppm) of CO_2 in dry air. This concentration is ≈13 times above the ambient level of 395 μmol/mol. Shown in the top panel of Fig. 4 are the averaged pulse sequence data from the reference detector (top trace) and signal detector (bottom trace) over a 25 μs time period. For matched cable lengths, the time delay of the signal pulse sequence relative to the reference sequence is 150(2) ns and gives a cell path length difference of 44.6(6) m (after accounting for the 0.4 m difference outside the cell). This measure of path length will be useful for path integrated concentration determinations in remote sensing applications.

The integrated signals from the signal and reference channels' pulse sequences are shown in the top two traces in the lower panel. The integration regions for all pulses in each sequence are 100 ns in width and separated by 200 ns. As discussed above, the sideband powers in the reference channel are leveled and vary by less than 2% except near the two ends of the scans. The corresponding absorption spectrum is shown in the lower part of Fig. 4. The absorbance is calculated from the negative natural logarithm of the normalized transmission signal. The signal is shown after subtraction of a small offset and sloping baseline obtained from the fit, and three standing wave interference components (commonly referred to as etalon fringes) arising from beam spot overlap in the White cell. The line intensity, center frequency, and Lorentzian width from pressure broadening were varied in the Voigt line shape [30] fit, while the small Gaussian component corresponding to the Doppler contribution was fixed to 0.347 GHz. The residuals from the best-fit Voigt profile are shown as the lowest trace. The integrated intensity is within 6% of model predictions from HITRAN [29], and the pressure broadened width of 4.36(1) GHz is in good agreement with the HITRAN value of 4.28 GHz. The slightly larger observed width may be a result of the small amount of light leakage that occurs across the frequency intervals as discussed above. From the root-mean-square noise of the residuals over the region of the line in Fig. 4 (and from other data discussed below), we estimate the detection sensitivity is $\approx 3 \times 10^{-9}$ $cm^{-1}\,Hz^{-1/2}$. It is further noted that the residuals across each 2000 sequence average have similar structures, suggesting smaller contributions from etalon fringes still remain.

With this sensitivity, ambient levels of CO_2 at 395 μmol/mol are within the detection limit for a single 25 μs scan. The fractional absorption of this line is expected to be small, near 0.3% for this concentration and path length, and therefore, the line profile was fixed and the integrated intensity and baseline were varied. It was also important in the fits to vary the phase shift of the etalon fringe patterns. The magnitude of the pattern can be comparable to the ambient level absorption strengths and depends strongly on the beam alignment through the cell. The time dependence of the phase shift depends on the delay following the gas fill as the stress across the cell relaxes from vacuum conditions. These simple corrections to the baseline would not have been possible if not for the rapid scan speed and ≈40 GHz of frequency coverage possible with this instrument.

Shown in Fig. 5(a) are the Allan deviations (square root of the Allan variances [31]) in log/log form for the best-fit intensities over a sequence of 40,000 scans (20,000 scan intervals) at ambient levels of CO_2, where the $k = 1$ (1σ) standard uncertainty of any individual scan is 220 μmol/mol. The data closely follow the line shown with slope of −1/2 for most of the 15 s collection time (1 s real time) as expected for an ergodic $n^{-1/2}$ improvement in S/N where n is the number of samples. Some break in the trend can be seen near the 10^3 sample interval, as this represents slight changes in the deviation occurring over the 0.7 s time gap between each of the segment acquisitions (each of the 20 segments contain 2000 consecutive scans acquired at a rate of 40 kHz). As a further confirmation of the system performance, a similar set of scans was acquired for a CO_2 gas mixture at 3900 μmol/mol (≈10× ambient level). The Allan deviations are shown in Fig. 5(b), and the corresponding best-fit integrated intensities are shown in Fig. 5(c). From Fig. 5(b), a similar trend in the S/N scaling with sample number is seen to hold at this higher concentration. Over the full data sets of Figs. 5(a) and 5(b), the measured uncertainties ($k = 1$ or 1σ) are 1.1 and 1.2 μmol/mol (ppm), respectively.

B. Direct Absorption of CH_4 Near 1.645 μm

As a demonstration of the broad tunability of the spectrometer, a similar study was performed on the *R*-branch lines of the overtone band ($2\nu_3$) of methane centered near 1643 nm using the same configuration. The CH_4 multiplet at (6086.633 – 6086.831) cm^{-1} (R7 line) is useful for concentration profiling using remote sensing methods [32] since it is one of the strongest lines in the band and is nearly free of water vapor interference. This region is also more than 40 nm to the red of the CO_2 region studied above. The broad tunability of this system permits a rapid change between these two regions in less than a few minutes. A wavemeter is used to accurately position the diode laser frequency using the grating control,

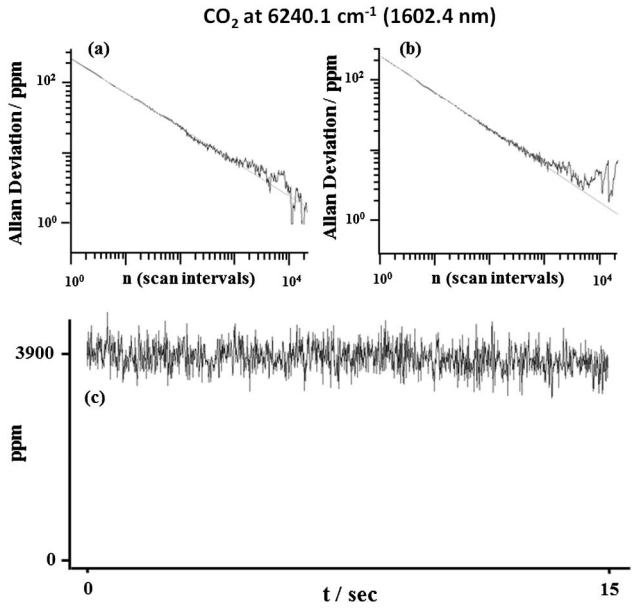

Fig. 5. Allan deviations in log/log form of the best-fit intensities obtained from the least-squares fits to a series of 25 μs scans over the CO_2 line at 1602.5 nm [29] for (a) ambient CO_2 in room air and (b) 3900 μmol/mol CO_2/dry air gas mixture. The corresponding line intensities for each single scan of (b) are shown in (c). The uncertainties in (a) decrease by ≈10-fold relative to (b) in accord with the 10-fold increase in concentration. Both data sets are in good agreement with the $n^{-1/2}$ signal-to-noise ratio improvement (line with slope of −1/2) with scan number n up to 1000. This sample number corresponds to the time for a sequential acquisition before scope-to-computer data transfer. Small deviations from ideal scaling are seen to occur for averaging times that extend over the 40,000 scans or 20 segments acquired. The data record corresponds to 1 s of acquisition time, although it is currently limited to 15 s because of the data throughput speed. The measurement uncertainty of the CO_2 concentration over this period is ±2 μmol/mol (ppm).

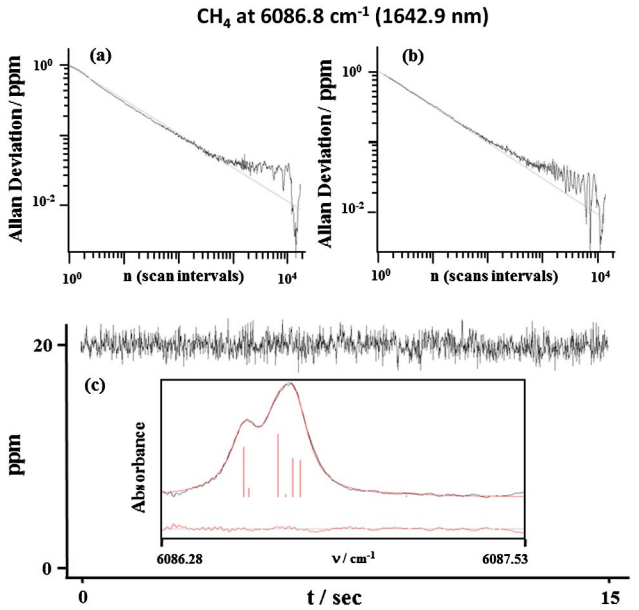

Fig. 6. Allan deviations in log/log form of the best-fit intensities obtained from the least-squares fits to a series of 25 μs scans over the CH_4 line at 1642.9 nm [29,32] for (a) ambient CH_4 in room air and (b) for a 20 μmol/mol CH_4/N_2 gas mixture. The corresponding integrated line intensities for each scan of (b) are shown in (c). The uncertainties in (a) decrease by ≈10-fold relative to (b) in accord with the 10-fold increase in concentration. The measurement uncertainty of the CH_4 concentration over this period is ±10 nmol/mol (ppb).

and the computer interface finely tunes the diode PZT control to bring its frequency into resonance with a mode of the filter cavity and then with a mode of the HeNe stabilized reference cavity. Once the frequency locks are established, a recalibration of the MW power driving the EOM is performed in less than a minute to level the sideband powers across the scan as described above (or a previously recorded calibration curve may be transferred to the AWG). Any diode laser frequency drift from hysteresis in the controls after a wavelength change is actively offset by reference cavity feedback to the diode PZT control. The diode laser has ≈2-fold less power near 1643 nm, although this is offset to some extent by the slightly higher gain of the amplifier.

The methane line at 6086.9 cm^{-1} has five main components that are unresolved at atmospheric pressure to give an asymmetric split profile shown as an inset in Fig. 6(c). In contrast to the high atmospheric concentration of CO_2 (≈395 μmol/mol), the atmospheric abundance of CH_4 is only 1.87 μmol/mol [33]. However, the lower concentration is almost completely offset by a 200-fold increase in the absorption strength for the line targeted at 1.645 μm. So, ambient levels of CH_4 will fall within the detection limit for a single 25 μs scan.

Room air was used to fill the White cell to 98.4 kPa (738 Torr) for the ambient level measurements. The Allan deviations determined from the best-fit integrated line intensities over a sequence of 40 000 scans are shown in the top panel of Fig. 6(a), where the $k = 1$ (1σ) standard uncertainty of the average over the individual scan intervals is 0.9 μmol/mol. The data lie near the ergodic decay line for up to 10^3 samples and show some increase for times over the different segments but improve again for the longest times. A similar set was obtained for a CH_4 gas mixture at 20 μmol/mol (≈10 times ambient level). Given the low concentration, the gas mixture was prepared in two dilution stages beginning with a premixed 310 μmol/mol gas sample containing high-purity CH_4 in high-purity N_2. After a few hours of mixing time, the cell was then filled with 6.67 kPa of the mixture and backfilled to 100 kPa (750 Torr). The Allan deviations shown in Fig. 6(b) for the 20 μmol/mol mixture were determined from best-fit intensities of Fig. 6(c). Similar to the trends observed for CO_2, the measured uncertainties for the Allan deviation show good agreement with the $n^{-1/2}$ line at both concentrations. Over the full set of scans in Figs. 6(a) and 6(b), the measured uncertainties ($k = 1$ or 1σ) are 4.8 and 3.8 nmol/mol (ppm), respectively.

Given the importance of fast monitoring of trace levels of CH_4 for remote sensing and in many enclosed environments to ensure concentrations do not exceed the lower explosive limit of 5%, the acquisition software was optimized to perform real-time monitoring of CH_4 under fast flow conditions in the multipass cell. The method of air injection through the cell is expected to lead to turbulent conditions as might be expected in the open atmosphere [20,21]. Easy visual detection of the CH_4 line with a S/N of ≈25:1 was obtained for a 200 sample average corresponding to a 5 ms time record. Since the data throughput is currently limited to 2000 scans in a 0.75 s interval, a continuous real-time update of the CH_4 concentration is demonstrated at 13 Hz. The single scan sensitivity is currently limited by the 8-bit resolution of the digitizer. Data acquisition hardware is now commercially available to

achieve the maximum throughput rate of 40 kHz with 16 bits of resolution and is expected to give a further improvement in the detection sensitivity.

4. CONCLUSIONS

A rapid and precise single-frequency step-scan method operating over the region from (1.59 to 1.65) μm is demonstrated for direct absorption detection of CO_2 and CH_4 at ambient levels in a 50 m multipass cell. The method is based on the sequential selection of a single sideband from an arbitrary-waveform-generator-driven electro-optic phase modulator (EOM) across a comb of frequencies transmitted by a low-finesse confocal resonator. The technique is shown to cover 123 discrete frequencies separated by 300 MHz across a 36.9 GHz region in a 25 μs scan time using the second-order sidebands of the EOM. The spectral range and resolution are more than needed to capture the full line shape profile of a gas at ambient pressure and the off-resonance baseline to allow for the removal of standing wave interference patterns (etalon fringes) arising from residual beam overlap in the multipass cell and from other stray reflections in the transmission path.

For atmospheric remote sensing studies, the 123 frequency intervals are in excess of what is needed to obtain reliable concentration measurements. Reduction to 10 frequencies measured in a 2 μs interval and distributed (perhaps asymmetrically) across a 30 GHz region should be adequate for concentration retrievals and spectral width determinations when probing regions with large pressure variation [23,24]. Under these conditions, a (2, 3) ms integration time is sufficient to achieve signal-to-noise ratios of >35:1 for CO_2 and CH_4. Furthermore, for distributed area monitoring, a spatial resolution of 100 m (200 m double passed) will be adequate to identify CO_2 leaks from sequestration sites and CH_4 emission from landfills, livestock pastures, and pipelines, providing another four-fold improvement in sensitivity to give detection limits that are less than 1% of their respective ambient level concentrations.

Extension of this method to broader spectral ranges that exceed 100 GHz is currently under development using higher-order modes of the EOM and with the use of an amplifier-multiplier chain (2X–4X) on the output of the AWG [17].

ACKNOWLEDGMENTS

Support was provided by the NIST Greenhouse Gas Measurements and Climate Research Program. G.-W. Truong was supported at NIST by an Australian Fulbright Fellowship.

REFERENCES

1. B. A. Paldus and A. A. Kachanov, "An historical overview of cavity-enhanced methods," Can. J. Phys. **83**, 975–999 (2005).
2. D. A. Long, A. Cygan, R. D. van Zee, M. Okumura, C. E. Miller, D. Lisak, and J. T. Hodges, "Frequency-stabilized cavity ring-down spectroscopy," Chem. Phys. Lett. **536**, 1–8 (2012).
3. J. T. Hodges, H. P. Layer, W. W. Miller, and G. E. Scace, "Frequency-stabilized single-mode cavity ring-down apparatus for high-resolution absorption spectroscopy," Rev. Sci. Instrum. **75**, 849–863 (2004).
4. R. Z. Martinez, M. Metsala, O. Vaittinen, T. Lantta, and L. Halonen, "Laser-locked, high-repetition-rate cavity ringdown spectrometer," J. Opt. Soc. Am. B **23**, 727–740 (2006).
5. J. Ye, L. S. Ma, and J. L. Hall, "Ultrasensitive detections in atomic and molecular physics: demonstration in molecular overtone spectroscopy," J. Opt. Soc. Am. B **15**, 6–15 (1998).
6. L. Gianfrani, R. W. Fox, and L. Hollberg, "Cavity-enhanced absorption spectroscopy of molecular oxygen," J. Opt. Soc. Am. B **16**, 2247–2254 (1999).
7. C. Ishibashi and H. Sasada, "Highly sensitive cavity-enhanced sub-Doppler spectroscopy of a molecular overtone band with a 1.66 μm tunable diode laser," Jpn. J. Appl. Phys. **38**, 920–922 (1999).
8. P. Ehlrs, I. Silander, J. Wang, and O. Axner, "Fiber-laser-based noise-immune cavity-enhanced optical heterodyne molecular spectrometry instrumentation for Doppler-broadened detection in the 10^{-12} cm^{-1} $Hz^{-1/2}$ region," J. Opt. Soc. Am. B **29**, 1305–1315 (2012).
9. A. Foltynowicz, F. M. Schmidt, W. Ma, and O. Axner, "Noise-immune cavity-enhanced optical heterodyne molecular spectrometry: current status and future potential," Appl. Phys. B **92**, 313–326 (2008).
10. K. O. Douglass, S. E. Maxwell, D. A. Long, J. T. Hodges, and D. F. Plusquellic, "Fast switching arbitrary frequency light source for broadband spectroscopic applications," U.S. patent 13/827,476 (March 14, 2013).
11. G.-W. Truong, K. O. Douglass, S. E. Maxwell, R. D. van Zee, D. F. Plusquellic, J. T. Hodges, and D. A. Long, "Frequency-agile, rapid scanning spectroscopy," Nat. Photonics **7**, 532–534 (2013).
12. D. A. Long, G.-W. Truong, R. D. van Zee, D. F. Plusquellic, and J. T. Hodges, "Frequency-agile, rapid scanning spectroscopy: absorption sensitivity of 2×10^{-12} cm^{-1} $Hz^{-1/2}$ with a tunable diode laser," Appl. Phys. B (posted August 3, 2013, in press).
13. J. U. White, "Long optical paths of large aperture," J. Opt. Soc. Am. **32**, 285–288 (1942).
14. D. R. Herriot, H. Kogelnik, and R. Kompfner, "Off-axis paths in spherical mirror interferometers," Appl. Opt. **3**, 523–526 (1964).
15. T. E. L. Smith, M. J. Wooster, M. Tattaris, and D. W. T. Griffith, "Absolute accuracy and sensitivity analysis of OP-FTIR retrievals of CO_2, CH_4 and CO over concentrations representative of "clean air" and "polluted plumes"," Atmos. Meas. Tech. **4**, 97–116 (2011).
16. K. L. Haller and P. C. D. Hobbs, "Double beam laser absorption spectroscopy: shot noise-limited performance at baseband with a novel electronic noise canceller," Proc. SPIE **1435**, 298–309 (1991).
17. E. Gerecht, K. O. Douglass, and D. F. Plusquellic, "Chirped-pulse terahertz spectroscopy for broadband trace gas sensing," Opt. Express **19**, 8973–8984 (2011).
18. S. Davis, M. Farnik, D. Uy, and D. J. Nesbitt, "Concentration modulation spectroscopy with a pulsed slit supersonic discharge expansion source," Chem. Phys. Lett. **344**, 23–30 (2001).
19. L. Nugent-Glandorf, T. Neely, F. Adler, A. J. Fleisher, K. C. Cossel, B. Bjork, T. Dinneen, J. Ye, and S. A. Diddams, "Mid-infrared virtually imaged phased array spectrometer for rapid and broadband trace gas detection," Opt. Lett. **37**, 3285–3287 (2012).
20. S. Kameyama, M. Imaki, Y. Hirono, S. Ueno, S. Kawakami, D. Sakaizawa, and M. Nakajima, "Performance improvement and analysis of a 1.6 μm continuous-wave modulation laser absorption spectrometer system for CO_2 sensing," Appl. Opt. **50**, 1560–1569 (2011).
21. D. Sakaizawa, C. Nagasawa, T. Nagai, M. Abo, Y. Shibata, M. Nakazato, and T. Sakai, "Development of a 1.6 micron differential absorption lidar with a quasi-phase-matching optical parametric oscillator and photon-counting detector for the vertical CO_2 profile," Appl. Opt. **48**, 748–757 (2009).
22. L. C. Andrews and R. L. Phillips, *Laser Beam Propagation through Random Media*, 2nd ed. (SPIE, 2005).
23. H. Riris, K. Numata, S. Li, S. Wu, A. Ramanathan, M. Dawsey, J. Mao, R. Kawa, and J. B. Abshire, "Airborne measurements of atmospheric methane column abundance using a pulsed integrated-path differential absorption lidar," Appl. Opt. **51**, 8296–8305 (2012).
24. K. Numata, J. R. Chen, S. T. Wu, and J. B. Abshire, "Frequency stabilization of distributed-feedback laser diodes at 1572 nm for lidar measurements of atmospheric carbon diode," Appl. Opt. **50**, 1047–1056 (2011).

25. R. W. P. Drever, J. L. Hall, F. V. Kowalski, J. Hough, G. M. Ford, A. J. Munley, and H. Ward, "Laser phase and frequency stabilization using an optical resonator," Appl. Phys. B **31**, 97–105 (1983).
26. D. F. Plusquellic, S. R. Davis, and F. Jahanmir, "Probing nuclear quadrupole interaction in the rotationally resolved $S_1 \leftarrow S_0$ electronic spectrum of 2-chloronaphthalene," J. Chem. Phys. **115**, 225–235 (2001).
27. E. Riedle, S. H. Ashworth, J. T. Farrell, Jr., and D. J. Nesbitt, "Stabilization and precise calibration of a continuous-wave difference frequency spectrometer by use of a simple transfer cavity," Rev. Sci. Instrum. **65**, 42–48 (1994).
28. V. B. Podobedov, D. F. Plusquellic, and G. T. Fraser, "THz laser study of self-pressure and temperature broadening and shifts of water lines for pressures up to 1.4 kPa," J. Quant. Spectrosc. Radiat. Transfer **87**, 377–385 (2004).
29. L. S. Rothman, I. E. Gordon, A. Barbe, D. Chris Benner, P. F. Bernath, M. Birk, L. R. Brown, A. Campargue, J.-P. Champion, K. Chance, L. H. Coudert, V. Dana, V. M. Devi, S. Fally, J.-M. Flaud, R. R. Gamache, A. Goldman, D. Jacquemart, I. Kleiner, N. Lacome, W. J. Lafferty, J. Y. Mandin, S. T. Massie, S. N. Mikhailenko, C. E. Miller, N. Moazzen-Ahmadi, O. V. Naumenko, A. V. Nikitin, J. Orphal, V. I. Perevalov, A. Perrin, A. Predoi-Cross, C. P. Rinsland, M. Rotger, M. Simeckova, M. A. H. Smith, K. Sung, S. A. Tashkun, J. Tennyson, R. A. Toth, A. C. Vandaele, and J. Vander Auwera, "The HITRAN 2008 molecular spectroscopic database," J. Quant. Spectrosc. Radiat. Transfer **110**, 533–572 (2009).
30. M. R. Zaghloul and A. N. Ali, "Algorithm 916: computing the Faddeyeva and Voigt functions," ACM Trans. Math. Softw. **38**, 1–22 (2011).
31. D. W. Allan, "Statistics of atomic frequency standards," Proc. IEEE **54**, 221–230 (1966).
32. C. Frankenberg, T. Warneke, A. Butz, I. Aben, F. Hase, P. Spietz, and L. R. Brown, "Methane spectroscopy in the near infrared and its implications on atmospheric retrievals," Atmos. Chem. Phys. Discuss. **8**, 10021–10055 (2008).
33. E. J. Dlugokencky, S. Houweling, L. Bruhwiler, K. A. Masarie, P. M. Lang, J. B. Miller, and P. P. Tans, "Atmospheric methane levels off: temporary pause or new steady state?" Geophys. Res. Lett. **30**, 1–4 (2003).